



The NANOGrav 15yr Data Set: Harmonic Analysis of the Pulsar Angular Correlations

Gabriella Agazie¹, Akash Anumarpudi¹, Anne M. Archibald², Zaven Arzoumanian³, Jeremy G. Baier⁴, Paul T. Baker⁵, Bence Bécsy⁴, Laura Blecha⁶, Kimberly K. Boddy⁷, Adam Brazier^{8,9}, Paul R. Brook¹⁰, Sarah Burke-Spolaor^{11,12,68}, Rand Burnette⁴, J. Andrew Casey-Clyde¹³, Maria Charisi¹⁴, Shami Chatterjee⁸, Tyler Cohen¹⁵, James M. Cordes⁸, Neil J. Cornish¹⁶, Fronefield Crawford¹⁷, H. Thankful Cromartie^{18,72}, Kathryn Crowter¹⁹, Megan E. DeCesar^{20,72}, Paul B. Demorest²¹, Heling Deng⁴, Lankeswar Dey^{11,12}, Timothy Dolch^{22,23}, Elizabeth C. Ferrara^{24,25,26}, William Fiore^{11,12}, Emmanuel Fonseca^{11,12}, Gabriel E. Freedman¹, Emiko C. Gardiner²⁷, Nate Garver-Daniels^{11,12}, Peter A. Gentile^{11,12}, Kyle A. Gersbach¹⁴, Joseph Glaser^{11,12}, Deborah C. Good²⁸, Kayhan Gültekin²⁹, Jeffrey S. Hazboun⁴, Ross J. Jennings^{11,12,69}, Aaron D. Johnson^{1,30}, Megan L. Jones¹, David L. Kaplan¹, Luke Zoltan Kelley²⁷, Matthew Kerr³¹, Joey S. Key³², Nima Laal⁴, Michael T. Lam^{33,34,35}, William G. Lamb¹⁴, Bjorn Larsen³⁶, T. Joseph W. Lazio³⁷, Natalia Lewandowska³⁸, Tingting Liu^{11,12}, Duncan R. Lorimer^{11,12}, Jing Luo^{39,70}, Ryan S. Lynch⁴⁰, Chung-Pei Ma^{27,41}, Dustin R. Madison⁴², Alexander McEwen¹, James W. McKee⁴³, Maura A. McLaughlin^{11,12}, Natasha McMann¹⁴, Bradley W. Meyers^{19,44}, Patrick M. Meyers³⁰, Chiara M. F. Mingarelli³⁶, Andrea Mitridate⁴⁵, Jonathan Nay⁷, Cherry Ng⁴⁶, David J. Nice⁴⁷, Stella Koch Ocker^{30,48}, Ken D. Olum⁴⁹, Timothy T. Pennucci⁵⁰, Benetge B. P. Perera⁵¹, Polina Petrov¹⁴, Nihan S. Pol⁵², Henri A. Radovan⁵³, Scott M. Ransom⁵⁴, Paul S. Ray³¹, Jessie C. Runnoe¹⁴, Alexander Saffer^{54,69}, Shashwat C. Sardesai¹, Ann Schmiedekamp⁵⁵, Carl Schmiedekamp⁵⁵, Kai Schmitz⁵⁶, Brent J. Shapiro-Albert^{11,12,57}, Xavier Siemens^{1,4}, Joseph Simon^{58,71}, Magdalena S. Siwek⁵⁹, Tristan L. Smith⁶⁰, Sophia V. Sosa Fiscella^{34,35}, Ingrid H. Stairs¹⁹, Daniel R. Stinebring⁶¹, Kevin Stovall²¹, Abhimanyu Susobhanan⁶², Joseph K. Swiggum^{47,69}, Jacob Taylor⁴, Stephen R. Taylor¹⁴, Jacob E. Turner⁴⁰, Caner Unal^{63,64,65}, Michele Vallisneri^{30,37}, Rutger van Haasteren⁶², Sarah J. Vigeland¹, Haley M. Wahl^{11,12}, Caitlin A. Witt^{66,67}, David Wright⁴, Olivia Young^{34,35}, and The NANOGrav Collaboration

¹ Center for Gravitation, Cosmology and Astrophysics, Department of Physics, University of Wisconsin-Milwaukee, P.O. Box 413, Milwaukee, WI 53201, USA
² Newcastle University, Newcastle, NE1 7RU, UK

³ X-Ray Astrophysics Laboratory, NASA Goddard Space Flight Center, Code 662, Greenbelt, MD 20771, USA

⁴ Department of Physics, Oregon State University, Corvallis, OR 97331, USA

⁵ Department of Physics and Astronomy, Widener University, One University Place, Chester, PA 19013, USA

⁶ Physics Department, University of Florida, Gainesville, FL 32611, USA

⁷ Department of Physics, The University of Texas at Austin, Austin, TX 78712, USA; jonathan.nay@nanograv.org

⁸ Cornell Center for Astrophysics and Planetary Science and Department of Astronomy, Cornell University, Ithaca, NY 14853, USA

⁹ Cornell Center for Advanced Computing, Cornell University, Ithaca, NY 14853, USA

¹⁰ Institute for Gravitational Wave Astronomy and School of Physics and Astronomy, University of Birmingham, Edgbaston, Birmingham, B15 2TT, UK

¹¹ Department of Physics and Astronomy, West Virginia University, P.O. Box 6315, Morgantown, WV 26506, USA

¹² Center for Gravitational Waves and Cosmology, West Virginia University, Chestnut Ridge Research Building, Morgantown, WV 26505, USA

¹³ Department of Physics, University of Connecticut, 196 Auditorium Road, U-3046, Storrs, CT 06269-3046, USA

¹⁴ Department of Physics and Astronomy, Vanderbilt University, 2301 Vanderbilt Place, Nashville, TN 37235, USA

¹⁵ Department of Physics, New Mexico Institute of Mining and Technology, 801 Leroy Place, Socorro, NM 87801, USA

¹⁶ Department of Physics, Montana State University, Bozeman, MT 59717, USA

¹⁷ Department of Physics and Astronomy, Franklin & Marshall College, P.O. Box 3003, Lancaster, PA 17604, USA

¹⁸ National Research Council Research Associate, National Academy of Sciences, Washington, DC 20001, USA

¹⁹ Department of Physics and Astronomy, University of British Columbia, 6224 Agricultural Road, Vancouver, BC V6T 1Z1, Canada

²⁰ George Mason University, Fairfax, VA 22030, USA

²¹ National Radio Astronomy Observatory, 1003 Lopezville Road, Socorro, NM 87801, USA

²² Department of Physics, Hillsdale College, 33 E. College Street, Hillsdale, MI 49242, USA

²³ Eureka Scientific, 2452 Delmer Street, Suite 100, Oakland, CA 94602-3017, USA

²⁴ Department of Astronomy, University of Maryland, College Park, MD 20742, USA

²⁵ Center for Research and Exploration in Space Science and Technology, NASA/GSFC, Greenbelt, MD 20771, USA

²⁶ NASA Goddard Space Flight Center, Greenbelt, MD 20771, USA

²⁷ Department of Astronomy, University of California, Berkeley, 501 Campbell Hall #3411, Berkeley, CA 94720, USA

²⁸ Department of Physics and Astronomy, University of Montana, 32 Campus Drive, Missoula, MT 59812, USA

²⁹ Department of Astronomy and Astrophysics, University of Michigan, Ann Arbor, MI 48109, USA

³⁰ Division of Physics, Mathematics, and Astronomy, California Institute of Technology, Pasadena, CA 91125, USA

³¹ Space Science Division, Naval Research Laboratory, Washington, DC 20375-5352, USA

³² University of Washington Bothell, 18115 Campus Way NE, Bothell, WA 98011, USA

³³ SETI Institute, 339 N Bernardo Ave Suite 200, Mountain View, CA 94043, USA

³⁴ School of Physics and Astronomy, Rochester Institute of Technology, Rochester, NY 14623, USA

³⁵ Laboratory for Multiwavelength Astrophysics, Rochester Institute of Technology, Rochester, NY 14623, USA

³⁶ Department of Physics, Yale University, New Haven, CT 06520, USA

³⁷ Jet Propulsion Laboratory, California Institute of Technology, 4800 Oak Grove Drive, Pasadena, CA 91109, USA

³⁸ Department of Physics and Astronomy, State University of New York at Oswego, Oswego, NY 13126, USA

³⁹ Department of Astronomy & Astrophysics, University of Toronto, 50 Saint George Street, Toronto, ON M5S 3H4, Canada

⁴⁰ Green Bank Observatory, P.O. Box 2, Green Bank, WV 24944, USA

⁴¹ Department of Physics, University of California, Berkeley, 366 Physics North MC 7300, Berkeley, CA 94720, USA

⁴² Department of Physics, University of the Pacific, 3601 Pacific Avenue, Stockton, CA 95211, USA

⁴³ Department of Physics and Astronomy, Union College, Schenectady, NY 12308, USA

- ⁴⁴ International Centre for Radio Astronomy Research, Curtin University, Bentley, WA 6102, Australia
⁴⁵ Deutsches Elektronen-Synchrotron DESY, Notkestr. 85, 22607 Hamburg, Germany
⁴⁶ Dunlap Institute for Astronomy and Astrophysics, University of Toronto, 50 St. George Street, Toronto, ON M5S 3H4, Canada
⁴⁷ Department of Physics, Lafayette College, Easton, PA 18042, USA
⁴⁸ The Observatories of the Carnegie Institution for Science, Pasadena, CA 91101, USA
⁴⁹ Institute of Cosmology, Department of Physics and Astronomy, Tufts University, Medford, MA 02155, USA
⁵⁰ Institute of Physics and Astronomy, Eötvös Loránd University, Pázmány P. s. 1/A, 1117 Budapest, Hungary
⁵¹ Arecibo Observatory, HC3 Box 53995, Arecibo, PR 00612, USA
⁵² Department of Physics, Texas Tech University, Box 41051, Lubbock, TX 79409, USA
⁵³ Department of Physics, University of Puerto Rico, Mayagüez, PR 00681, USA
⁵⁴ National Radio Astronomy Observatory, 520 Edgemont Road, Charlottesville, VA 22903, USA
⁵⁵ Department of Physics, Penn State Abington, Abington, PA 19001, USA
⁵⁶ Institute for Theoretical Physics, University of Münster, 48149 Münster, Germany
⁵⁷ Giant Army, 915A 17th Ave, Seattle, WA 98122, USA
⁵⁸ Department of Astrophysical and Planetary Sciences, University of Colorado, Boulder, CO 80309, USA
⁵⁹ Center for Astrophysics, Harvard University, 60 Garden St, Cambridge, MA 02138, USA
⁶⁰ Department of Physics and Astronomy, Swarthmore College, Swarthmore, PA 19081, USA
⁶¹ Department of Physics and Astronomy, Oberlin College, Oberlin, OH 44074, USA
⁶² Max-Planck-Institut für Gravitationsphysik (Albert-Einstein-Institut), Callinstrasse 38, D-30167, Hannover, Germany
⁶³ Department of Physics, Middle East Technical University, 06531 Ankara, Turkey
⁶⁴ Department of Physics, Ben-Gurion University of the Negev, Be'er Sheva 84105, Israel
⁶⁵ Feza Gursey Institute, Bogazici University, Kandilli, 34684, Istanbul, Turkey
⁶⁶ Center for Interdisciplinary Exploration and Research in Astrophysics (CIERA), Northwestern University, Evanston, IL 60208, USA
⁶⁷ Adler Planetarium, 1300 S. DuSable Lake Shore Dr., Chicago, IL 60605, USA

Received 2024 November 20; revised 2025 March 24; accepted 2025 April 3; published 2025 May 16

Abstract

Pulsar timing array observations have found evidence for an isotropic gravitational-wave background with the Hellings–Downs angular correlations between pulsar pairs. This interpretation hinges on the measured shape of the angular correlations, which is predominantly quadrupolar under general relativity. Here we explore a more flexible parameterization: we expand the angular correlations into a sum of Legendre polynomials and use a Bayesian analysis to constrain their coefficients with the 15 yr pulsar timing data set collected by the North American Nanohertz Observatory for Gravitational Waves (NANOGrav). When including Legendre polynomials with multipoles $\ell \geq 2$, we only find a significant signal in the quadrupole with an amplitude consistent with general relativity and nonzero at the $\sim 95\%$ confidence level and a Bayes factor of 200. When we include multipoles $\ell \leq 1$, the Bayes factor evidence for quadrupole correlations decreases by more than an order of magnitude due to evidence for a monopolar signal at approximately 4 nHz, which has also been noted in previous analyses of the NANOGrav 15 yr data. Further work needs to be done in order to better characterize the properties of this monopolar signal and its effect on the evidence for quadrupolar angular correlations.

Unified Astronomy Thesaurus concepts: [Gravitational waves \(678\)](#); [Gravitational wave astronomy \(675\)](#); [Millisecond pulsars \(1062\)](#); [Radio pulsars \(1353\)](#); [Supermassive black holes \(1663\)](#)

1. Introduction

Several independent pulsar timing array (PTA) observations have found evidence for a gravitational-wave background (GWB) in the nHz frequency band with high levels of significance (G. Agazie et al. 2023a; J. Antoniadis et al. 2023; D. J. Reardon et al. 2023; H. Xu et al. 2023). This GWB may have been produced by a population of unresolved supermassive black hole binaries (SMBHBs; G. Agazie et al. 2023b), exotic processes in the early universe that source a cosmological GWB (K. K. Boddy et al. 2022; R. Caldwell et al. 2022; D. Green et al. 2022), or a combination of both (A. Afzal et al. 2023).

PTA observations measure pulses of radio emission from millisecond pulsars, which serve as precise astronomical clocks due to their highly stable rotational periods (D. N. Matsakis et al. 1997; G. Hobbs et al. 2012, 2019). Gravitational waves (GWs) cause shifts in the pulse times of arrival (TOAs), and PTA observations achieve sensitivity to the effects of ~ 1 –100 nHz GWs by cross-correlating TOAs between pairs of pulsars (M. V. Sazhin 1978; S. L. Detweiler 1979; M. Maggiore 2018; C. M. F. Mingarelli & J. A. Casey-Clyde 2022). Furthermore, for an isotropic stochastic GWB, these cross-correlations are purely a function of the angular separation between the pairs of pulsars on the sky, and general relativity (GR) predicts that they should have a predominately quadrupolar angular correlation known as the Hellings–Downs (HD) curve (R. W. Hellings & G. S. Downs 1983).

The detection of a significant cross-correlation consistent with the HD curve is considered essential in order to claim the detection of a GWB (see, e.g., B. Allen et al. 2023). Deviations from this expectation may be due to mundane systematic effects such as errors in the solar system ephemerides, which create a time-dependent dipolar correlation (E. Roebber 2019; M. Vallisneri et al. 2020) or errors in the correction of the time at the telescope to a common inertial time, causing a time-

⁶⁸ Sloan Fellow.

⁶⁹ NANOGrav Physics Frontiers Center Postdoctoral Fellow.

⁷⁰ Deceased.

⁷¹ NSF Astronomy and Astrophysics Postdoctoral Fellow.

⁷² Resident at the U.S. Naval Research Laboratory, Washington, DC 20375, USA.



dependent monopolar correlation (G. Hobbs et al. 2012, 2019; see also C. Tiburzi et al. 2016; Z. Arzoumanian et al. 2020). In addition, measuring the angular power spectrum may help identify the presence of anisotropies in the GWB (C. M. F. Mingarelli et al. 2013; S. R. Taylor & J. R. Gair 2013; J. Gair et al. 2014; S. C. Hotinli et al. 2019; Y. Ali-Haïmoud et al. 2020). More exotic possibilities, like deviations from GR, also affect the detailed shape of the pulsar-pair angular correlations (K. J. Lee et al. 2008; S. J. Chamberlin & X. Siemens 2012; N. J. Cornish et al. 2018; Z. Arzoumanian et al. 2021).

The North American Nanohertz Observatory for Gravitational Waves (NANOGrav) collaboration has used its 15 yr pulsar timing data set to search for a GWB (G. Agazie et al. 2023a, hereafter NG15). The Bayesian analyses performed in NG15 and by other PTA collaborations (J. Antoniadis et al. 2023; D. J. Reardon et al. 2023; H. Xu et al. 2023) focused on establishing the evidence for the HD cross-correlations over an analysis that neglects the cross-correlations altogether. Here we use a more flexible parameterization of the shape of the angular cross-correlations by expanding it into a sum of Legendre polynomials with free coefficients c_ℓ ; we refer to this as a “harmonic analysis” (J. Nay et al. 2024). GR predicts the angular power spectrum has a dominant quadrupole ($\ell=2$) contribution due to the two tensor polarization modes of GWs, while higher multipole contributions scale as $\sim\ell^{-3}$ (J. Gair et al. 2014; W. Qin et al. 2019).

Consistent with the NG15 results and with the predictions of an isotropic GWB in GR, we find strong evidence (H. Jeffreys 1998; a Bayes factor of 200) for the dominant quadrupole correlations in the NANOGrav 15 yr data with $c_2/c_2^{\text{HD}} = 1.088_{-0.45}^{+0.32}$, and there is no evidence for multipoles higher than the quadrupole. When we include monopole correlations in our analyses, the quadrupole evidence is reduced by more than an order of magnitude due to the presence of a monopolar signal in the data at ≈ 4 nHz. This monopolar signal has been extensively investigated (A. Afzal et al. 2023; G. Agazie et al. 2023a) but currently has no clear explanation.

Previous work on parameterizing the shape of the pulsar-pair cross-correlations has focused on using a minimum variance estimator (i.e., the optimal statistic; M. Anholm et al. 2009; P. B. Demorest et al. 2013; S. J. Chamberlin et al. 2015; S. J. Vigeland et al. 2018). In particular, the multiple component optimal statistic (MCOS; S. C. Sardesai et al. 2023) allows for an estimate of the c_ℓ s that broadly agrees with the harmonic analysis we present here. The differences that we find are likely due to the fact that the current MCOS approach does not properly take into account the full cross-correlation between pulsars (see Section 4). Furthermore, some MCOS analyses that have appeared in the literature (e.g., NG15) account only for the uncertainty in the estimator itself, leaving out the much larger contribution due to marginalizing over the uncertainty in the GWB amplitude. Most importantly, the Bayesian analysis we present here directly utilizes the PTA likelihood when exploring the inferred shape of the angular cross-correlations expanded in Legendre polynomials.

The paper is organized as follows. In Section 2, we provide the background for our harmonic analysis approach, discuss our modeling methodologies, and list the various models we use in this paper. In Section 3, we provide the results of our GWB harmonic analyses on previous NANOGrav data sets,

investigate alternative monopole and dipole correlations, and examine frequency-dependent angular-correlation models. In Section 4, we compare our results to previous work parameterizing the shape of the pulsar-pair angular correlations, including the MCOS approach. We discuss our results and summarize our conclusions in Section 5.

2. Harmonic Analysis Methods

The Bayesian analysis of the NANOGrav 15 yr data is identical to what is done in NG15; in particular, the likelihood function is given by (A. D. Johnson et al. 2024)

$$p(\delta\mathbf{t} | \boldsymbol{\eta}) = \frac{1}{\sqrt{\det(2\pi\mathcal{C})}} \exp\left(-\frac{1}{2}\delta\mathbf{r}^T\mathcal{C}^{-1}\delta\mathbf{r}\right), \quad (1)$$

where $\delta\mathbf{t}$ are the pulsar timing residuals, $\boldsymbol{\eta}$ are the model parameters, and \mathcal{C} is a covariance matrix. The covariance matrix consists of several sources of white noise for each pulsar, whose parameters are set to the maximum likelihood of an analysis of individual pulsars (G. Agazie et al. 2023c). The residual vector is defined to be

$$\delta\mathbf{r} \equiv \delta\mathbf{t} - \mathcal{F}\mathbf{c} - \mathcal{M}\boldsymbol{\epsilon}, \quad (2)$$

where $\mathcal{F}\mathbf{c}$ is a Gaussian process that models intrinsic and correlated red-noise processes and $\mathcal{M}\boldsymbol{\epsilon}$ takes variations in the deterministic timing model for each pulsar into account. For our harmonic analysis, the dispersion measure (DM) is included in the deterministic timing model as a piecewise-constant function, referred to as DMX (Z. Arzoumanian et al. 2015; M. L. Jones et al. 2017), to be consistent with the main results of NG15. An alternate DM model explored in NG15 uses a stochastic Fourier-domain Gaussian process, referred to as DMGP (S. Chen et al. 2021; B. Goncharov et al. 2021; J. Antoniadis et al. 2022). The DMGP model prefers a GWB with smaller amplitude and steeper negative spectral slope when compared to the DMX model (see Figure 5 of NG15). However, the choice of DM model does not change the significance of the cross-correlations (see discussion in Section 5.1 of NG15), which is the focus of this paper.

The set of \mathbf{c} from Equation (2) is drawn from a zero-mean Gaussian with covariance

$$\langle c_{ai}c_{bj} \rangle = \delta_{ij}(\delta_{ab}\varphi_{a,i} + S_{ab,i}), \quad (3)$$

where a, b range over pulsars and i, j over Fourier components, which are then transformed into the time domain. The term $\varphi_{a,i}$ models the spectrum of intrinsic red noise in pulsar a , which is modeled as a power law,

$$P_{\text{RN},a}(f) \equiv \frac{A_{\text{RN},a}^2}{12\pi^2} \left(\frac{f}{f_{\text{yr}}}\right)^{-\gamma_{\text{RN},a}} f_{\text{yr}}^{-3}, \quad (4)$$

where $A_{\text{RN},a}$ is the dimensionless amplitude for the intrinsic red noise of pulsar a , and $\gamma_{\text{RN},a}$ is the corresponding spectral index. The term $S_{ab,i}$ models a stochastic process that is correlated across all pulsars, and the autocorrelation $S_{aa,i}$ is the same for all pulsars. We refer the reader to A. D. Johnson et al. (2024) for a more detailed discussion of the likelihood.

The correlated stochastic process can be expressed in the general form

$$S_{ab}(f) = P(f) \Gamma_{ab}(f), \quad (5)$$

where $P(f)$ is the frequency power spectrum, and $\Gamma_{ab}(f)$ is the angular-correlation function (which may, in general, depend on frequency). We follow the convention of referring to terms in our model as a cross-correlation when a and b denote distinct pulsars, and an autocorrelation when a and b denote the same pulsar.

We describe the specific angular-correlation parameterizations used in this paper in Section 2.1. We describe our frequency power-spectrum models in Section 2.2. The Bayesian analysis models used in this paper are provided in Section 2.3. Our method of calculating model evidence and individual angular-correlation evidence is described in Section 2.4.

2.1. GWB Angular-correlation Models

GR predicts that an isotropic stochastic GWB induces a frequency-independent angular correlation between pulsar pairs given by the HD curve (R. W. Hellings & G. S. Downs 1983)

$$\Gamma_{ab}^{\text{HD}} = (1 + \delta_{ab}) \left[\frac{1}{2} - \frac{1}{4} \left(\frac{1 - \cos \theta_{ab}}{2} \right) + \frac{3}{2} \left(\frac{1 - \cos \theta_{ab}}{2} \right) \log \left(\frac{1 - \cos \theta_{ab}}{2} \right) \right], \quad (6)$$

where $\cos \theta_{ab} = \hat{n}_a \cdot \hat{n}_b$ for pulsars a and b located on the sky at \hat{n}_a and \hat{n}_b , respectively, and δ_{ab} comes from the pulsar term, which is relevant for colocated pulsars (R. W. Hellings & G. S. Downs 1983; M. Anholm et al. 2009; C. M. F. Mingarelli et al. 2013).

An equivalent representation of the HD curve using a Legendre polynomial expansion gives the angular-correlation function (J. Gair et al. 2014; E. Roebber & G. Holder 2017)

$$\Gamma_{ab}^{\text{HD}} = (1 + \delta_{ab}) \sum_{\ell=2}^{\infty} c_{\ell}^{\text{HD}} P_{\ell}(\cos \theta_{ab}), \quad (7)$$

where P_{ℓ} are Legendre polynomials with coefficients

$$c_{\ell}^{\text{HD}} = \frac{3}{2} (2\ell + 1) \frac{(\ell - 2)!}{(\ell + 2)!} \quad (8)$$

for $\ell \geq 2$ and $c_0^{\text{HD}} = c_1^{\text{HD}} = 0$. The HD Legendre coefficients exhibit a dominant quadrupolar contribution and a sharp drop-off ($\propto \ell^{-3}$) at higher multipoles.

In order to extract information about the measured angular correlations, our harmonic analysis parameterization treats the cross-correlations separately from the autocorrelations (J. Nay et al. 2024)

$$\Gamma_{ab}^{\ell_{\text{max}}} = \delta_{ab} + (1 - \delta_{ab}) \sum_{\ell=2}^{\ell_{\text{max}}} c_{\ell} P_{\ell}(\cos \theta_{ab}), \quad (9)$$

where the first term in Equation (9) is the autocorrelation, normalized so that $\Gamma_{aa}^{\ell_{\text{max}}} = 1$, while the second term is the cross-correlation and is the parameterization of the HD angular-correlation function in Equation (7). Our parameterization splits the autocorrelations and cross-correlations into two distinct terms; there are both benefits and drawbacks to this approach.

The parameterization in Equation (9) allows us to directly test for the presence of cross-correlations, since in the limit that $c_{\ell} = 0$, we are left with only a contribution to the autocorrelation. As a result, a significant measurement of any c_{ℓ} is evidence for a nonzero cross-correlation. In addition, the inferred shape of the angular correlations comes solely from the pulsar cross-correlations, which are unaffected by processes that are intrinsic to each pulsar. Finally, this choice allows us to directly compare the constraints found here to previous methods used to characterize the shape of the angular correlations, which also exclusively rely on the pulsar cross-correlations (see Section 4). On the other hand, since any physical effect imposes a particular relationship between the autocorrelations and cross-correlations, our split analysis cannot be used to directly constrain those effects. Instead, our parameterization in Equation (9) provides a consistency check on the shape of the angular correlations.

Finally, we note that the parameterization in Equation (9) only contains multipoles with $\ell \geq 2$. This restriction is motivated by the expectation that the angular correlations described by these multipoles all share the same frequency power spectrum, $P(f)$ (see Equation (5)). Lower multipoles may be excited by nonstandard GW polarizations, unmodeled effects on the timing of the pulsars, and shifts in the solar system barycenter. Such effects, in general, come with a different dependence on time. Given this, we model these lower multipoles using a separate frequency power spectrum, as discussed in more detail in the next subsection and in Table 1.

2.2. Frequency Power-spectrum Models

We model the frequency power spectrum for the GWB as a power law:

$$P_{\text{gw}}(f) \equiv \frac{A_{\text{gw}}^2}{12\pi^2} \left(\frac{f}{f_{\text{yr}}} \right)^{-\gamma_{\text{gw}}} f_{\text{yr}}^{-3}, \quad (10)$$

where A_{gw} is the dimensionless strain amplitude of the GWB at a reference frequency $f_{\text{yr}} = 1/\text{yr}$, and γ_{gw} is the spectral index. We expect $\gamma_{\text{gw}} \simeq 13/3$ for a collection of inspiraling SMBHBs (E. S. Phinney 2001).

The frequency power spectrum for a monopole and dipole is modeled as an independent parameter for each GWB frequency. This approach is referred to as a ‘‘free-spectrum’’ model (e.g., see NG15). Using the same approach as in NG15, we define the free-spectrum parameter for the i th frequency

$$\Phi^2(f_i) \equiv P(f_i) \Delta f = P(f_i) / T_{\text{obs}}, \quad (11)$$

where Δf is the frequency resolution, which is set by T_{obs} , the longest observational baseline obtained by taking the difference between the first and last TOA measurement of the data set.

2.3. Bayesian Analysis Models

The baseline GWB harmonic analysis is the product of Equations (9) and (10), which gives

$$S_{ab}(f) = \frac{A_{\text{gw}}^2}{12\pi^2} \left(\frac{f}{f_{\text{yr}}} \right)^{-\gamma_{\text{gw}}} f_{\text{yr}}^{-3} \Gamma_{ab}^{\ell_{\text{max}}}. \quad (12)$$

We denote this model by HA $\gamma(c_2, \dots, c_{\ell_{\text{max}}})$.

Table 1 provides the models used in this paper, which are similarly obtained by multiplying an angular-correlation model

Table 1
List of Models Used in Our Analyses

Model Name	Model Description	Angular-correlation Parameterization	Frequency Power-spectrum Parameterization
HA $^\gamma(c_2, \dots, c_{\ell_{\max}})$	Parameterized angular correlations	$\Gamma_{ab}^{\ell_{\max}}$ (Equation (9))	$P_{\text{gw}}(f)$ (Equation (10))
HD $^\gamma$	Fixed HD angular correlations	Γ_{ab}^{HD} (Equation (7))	$P_{\text{gw}}(f)$
CURN $^\gamma$	Common uncorrelated red noise	$\Gamma_{ab}^{\text{CURN}} = \delta_{ab}$	$P_{\text{gw}}(f)$
IRN	Pulsar intrinsic red noise	$\Gamma_{ab}^{\text{IRN}} = \delta_{ab}$	$P_{\text{RN},a}(f)$ (Equation (4))
MONO $^{\text{free}}$	Monopole free spectrum	$\Gamma_{ab}^{\text{MONO}} = 1$	$\Phi^2(f)T_{\text{obs}}$ (Equation (11))
DIP $^{\text{free}}$	Dipole free spectrum	$\Gamma_{ab}^{\text{DIP}} = \cos \theta_{ab}$	$\Phi^2(f)T_{\text{obs}}$

Note. Each model is the product of the angular-correlation parameterization and the frequency power-spectrum parameterization listed above. The GWB harmonic analysis model in the first row, HA $^\gamma(c_\ell)$, comes from J. Nay et al. (2024) and is the primary model for this paper. The remaining models listed above follow the same naming convention as in NG15.

with a frequency power-spectrum model. The remaining models in Table 1 are the same as those used in NG15, and we use the same naming convention as NG15. In particular, for the CURN model, which assumes no angular correlations, and the HD model, we use a γ superscript to denote γ_{gw} is a model parameter. The pulsar intrinsic red-noise (IRN) model is included for every pulsar in each analysis.

2.4. Methods of Determining Evidence

We compute the model evidence by comparing the Bayesian evidence for two different models using product-space sampling (S. J. Goddard 2001; S. Hee et al. 2016; B. P. Carlin & S. Chib 2018) to determine the posterior odds ratio, as described in NG15 and A. D. Johnson et al. (2024). For this paper, all Bayes factors are calculated by performing a model comparison with either a CURN $^\gamma$ model or an HD $^\gamma$ model.

We use the Savage–Dickey Bayes factor method (J. M. Dickey 1971) to determine evidence for including a single multipole in our model. The Savage–Dickey Bayes factor for a model with a single multiple ℓ is (J. Nay et al. 2024)

$$\text{SD}_\ell = \frac{1}{p(c_\ell = 0)}, \quad (13)$$

where $p(c_\ell = 0)$ is the probability of the Legendre coefficient’s marginalized 1D posterior distribution evaluated at zero. As discussed in Appendix B of J. Nay et al. (2024), this approach is justified because the lower bound of the prior range for each c_ℓ is zero (see Section 3.1), and setting the Legendre coefficient to zero removes the parameter from the model, as seen in Equation (9).

3. Analyses and Results

We use ENTERPRISE (J. A. Ellis et al. 2020) and enterprise-extensions (S. R. Taylor et al. 2021) to calculate the likelihood function in Equation (1). We modify enterprise-extensions to include the Legendre coefficients as model parameters, as discussed in Section 2.1, which is the same modification used in J. Nay et al. (2024). We make additional modifications to enterprise-extensions to include free spectra models and frequency-dependent Legendre coefficient models discussed in Section 2.3. We also use the HyperModel module (referred to hereafter as hypermodel) of

enterprise-extensions to calculate Bayes factors between pairs of models. We use PTMCMCSampler (J. Ellis & R. van Haasteren 2017) to perform Markov chain Monte Carlo (MCMC) sampling to determine parameter posterior distributions.

In Section 3.1, we describe the data sets, the white noise modeling technique, and the parameters used in our harmonic analyses. In Section 3.2, we calculate the evidence for angular correlations in the NANOGrav data. In Section 3.3, we analyze the multipole posterior distributions and use our results to reconstruct the angular-correlation function. In Section 3.4, we extend our harmonic analyses to include monopole and dipole angular correlations.

3.1. Analysis Inputs and Parameters

We analyze the NG15 data set for the majority of the work presented in this paper. For comparison, we also analyze the NANOGrav 12.5 yr data set in Z. Arzoumanian et al. (2020, hereafter NG12.5). We use the same pulsars in our harmonic analyses as in the original NANOGrav GWB papers; in particular, we only include pulsars with an observation time span greater than 3 yr, which provides 67 and 45 pulsars for the NG15 and NG12.5 data sets, respectively.

For both the NG12.5 and NG15 data sets, we use the same number of frequencies ($N_f = 14$) for the GWB power spectrum as in their original analyses, with binned frequencies $f_i = i/T_{\text{obs}}$ for $i = 1, \dots, N_f$. For all analyses, including single pulsar noise modeling, we use $N_f = 30$ for the pulsar intrinsic red-noise power spectrum. For monopole and dipole free-spectrum models, we use $N_f = 5$, which covers the frequencies for which the evidence for a GWB is the strongest (as demonstrated in NG15).

The MCMC priors are given in Table 2. For the Legendre coefficients, the lower end of the prior range comes from the requirement that the angular power spectrum is strictly positive, as shown in Equation (8), while the upper end comes from the requirement that the full pulsar covariance be positive definite.

We note that in addition to the priors listed in Table 2, there is an implicit prior on the c_ℓ ’s due to their effect on the positive definiteness of the red-process covariance matrix given in Equation (3). If $\sum_{\ell=2}^{\ell_{\max}} c_\ell \gtrsim 1$, then the cross-correlations are larger than the GWB’s contribution to the autocorrelations for pulsar-pair separation angles near $\theta_{ab} = 0$. This can result in a red-process covariance matrix (Equation (3)) that is not positive

Table 2
Prior Ranges for the MCMC Parameters

MCMC Parameter	MCMC Prior Range	Bayesian Analysis Model
$\log_{10} A_{\text{gw}}$	$U[-18, -11]$	GWB power law
γ_{gw}	$U[0, 7]$	GWB power law
c_ℓ	$U[0, 1]$	Harmonic analysis
$\log_{10} \Phi(f_i)$	$U[-9, -4]$	Free spectrum
$\log_{10} A_{\text{RN},a}$	$U[-20, -11]$	Pulsar IRN
$\gamma_{\text{RN},a}$	$U[0, 7]$	Pulsar IRN

Note. We denote uniform ranges by $U[x_{\min}, x_{\max}]$.

definite. The Cholesky decomposition algorithm used by ENTERPRISE to find the inverse of this covariance matrix then fails for these parameter values. This constraint imposes a prior $\sum_{\ell=2}^{\ell_{\max}} c_\ell \leq 1$ so that the full prior on each Legendre coefficient is

$$p(x) = N_\ell(1 - x)^{N_\ell - 1}, \quad (14)$$

where N_ℓ is the total number of multipoles in the GWB model, and $x \in [0, 1]$.

We run multiple MCMC chains in parallel to reduce processing time, then we combine sampling chains after removing a 25% burn-in to create a single final chain. The sampling chains are run at the same temperature, because the trace-plots indicate good exploration of parameter space that is stationary between chains (as seen in the triangle plots of this section). We use the Gelman–Rubin R -statistic (A. Gelman & D. B. Rubin 1992) as a measure of sampling chain convergence and require $R - 1 < 0.05$ for all GWB parameters. In addition, we require the autocorrelation-to-chain length ratio to be < 0.01 for all GWB parameters.

3.2. Bayesian Evidences

For the NG15 data set, we find that the Bayes factor of an $\text{HA}(c_2)/\text{HD}^\gamma$ hypermodel is ≈ 1 , which implies there is no preference for a model with quadrupole-only correlations over a model with HD correlations. Table 3 provides the Bayes factors and information on the marginalized 1D posterior distributions for c_2 for various harmonic models, relative to a CURN^γ model. Notably, we find the Bayes factor of a $\text{HA}^\gamma(c_2)/\text{CURN}^\gamma$ hypermodel is ≈ 200 , consistent with the Bayes factor of ≈ 200 for an $\text{HD}^\gamma/\text{CURN}^\gamma$ hypermodel for 14 GWB frequency components found in NG15.

When we include multipoles higher than the quadrupole, the evidence is reduced. For $\ell_{\max} = 3, 4, \text{ and } 5$, the $\text{HA}^\gamma(c_2, \dots, c_{\ell_{\max}})/\text{CURN}^\gamma$ hypermodels give Bayes factors of approximately 55, 1, and 0.1, respectively. These results are consistent with no evidence for multipoles $\ell \geq 4$ in our model. The Bayes factor of 55 for an $\text{HA}(c_2, c_3)/\text{CURN}^\gamma$ hypermodel suggests some evidence that the octupole may be present in the data. However, from transitivity, we get a Bayes factor of approximately 3.6 for an $\text{HA}(c_2)/\text{HA}(c_2, c_3)$ hypermodel, meaning a model with quadrupole-only correlations is highly preferred over a model with quadrupole and octupole correlations. Moreover, the marginalized 1D posterior distribution for the octupole is consistent with zero (see Section 3.3).

For the NG12.5 data set, the Bayes factor of $\text{HA}^\gamma(c_2)/\text{CURN}^\gamma$ is ≈ 4 , consistent with the Bayes factors reported

Table 3
Summary of Bayes Factors and Quadrupole Statistics from Harmonic Analyses of the NG15 Data Set

Bayesian Model Name	Bayes Factor	Quadrupole (c_2)		
		Mean	68% CL	95% CL
$\text{HA}^\gamma(c_2)$	200	0.34	[0.20, 0.44]	[0.11, 0.58]
$\text{HA}^\gamma(c_2, c_3)$	55	0.30	[0.16, 0.41]	[0.07, 0.56]
$\text{HA}^\gamma(c_2, c_3, c_4)$	0.9	0.28	[0.14, 0.38]	[0.05, 0.52]
$\text{HA}^\gamma(c_2, \dots, c_5)$	0.1	0.27	[0.14, 0.36]	[0.05, 0.49]
$\text{HA}^\gamma(c_2)(45\text{psrs})$	170	0.33	[0.19, 0.44]	[0.10, 0.58]

Note. The Bayes factors are calculated relative to a CURN^γ model, which does not include angular correlations. The mean value of the quadrupole’s marginalized 1D posterior distribution is provided at the 68% and 95% CLs. The analysis in the last row uses the NG15 data set, but only includes the 45 pulsars in the NG12.5 data set.

in NG12.5 for $\text{HD}^\gamma/\text{CURN}^\gamma$. To understand the reason for the large jump in quadrupole evidence going from the NG12.5 data set to the NG15 data set, we perform an additional analysis in which we use the NG15 data set restricted to the 45 pulsars from the NG12.5 data set, denoted $\text{HA}^\gamma(c_2)(45\text{psrs})$. The Bayes factor of $\text{HA}^\gamma(c_2)(45\text{psrs})/\text{CURN}^\gamma$ is 170, which is nearly the same as $\text{HA}^\gamma(c_2)/\text{CURN}^\gamma$. Thus, the large change in quadrupole evidence from the NG12.5 data set to the NG15 data set is primarily due to increasing the observation time span of the longest observed pulsars. This result is not surprising because the 22 pulsars added between the NG12.5 and the NG15 data sets do not have long observation time spans, and therefore contribute less to lower frequencies where the GWB signal is expected to be the strongest.

3.3. Posterior Distributions

We show the marginalized 1D and 2D posterior distributions of the three GWB parameters from model $\text{HA}^\gamma(c_2)$ when fit to the NG15 data set in Figure 1. The posterior distribution of c_2 is consistent with the theoretical HD value of the quadrupole correlation, c_2^{HD} from Equation (8), denoted by the dashed line in Figure 1. The GWB amplitude and spectral index for an HD^γ model, which has angular correlations fixed to the theoretical HD values, is shown in gray. We can see that the posterior distribution for c_2 is negligibly correlated with γ_{gw} and $\log_{10} A_{\text{gw}}$.

The quadrupole’s posterior distribution broadens as the number of Legendre coefficients in the model increases, as evident from Table 3. However, even for $\ell_{\max} = 5$, the posterior distribution of c_2 is consistent with c_2^{HD} and is nonzero at the 95% confidence level (CL). The left panel of Figure 2 shows the marginalized 1D and 2D posterior distributions of the quadrupole and octupole from model $\text{HA}^\gamma(c_2, c_3)$; the posterior distribution for the octupole is consistent with zero and is representative of the posterior distributions of all higher multipoles when we include higher multipoles in the model.

Using Equation (9), we can reconstruct the angular-correlation function from the 68% and 95% contour regions of the marginalized 2D posterior distributions for c_2 and c_3 . The right panel of Figure 2 shows these reconstructions from the harmonic analyses of the NG12.5 and NG15 data sets with model $\text{HA}^\gamma(c_2, c_3)$. The dark- and light-shaded regions denote the 68% CL and 95% CL regions, respectively. The dashed

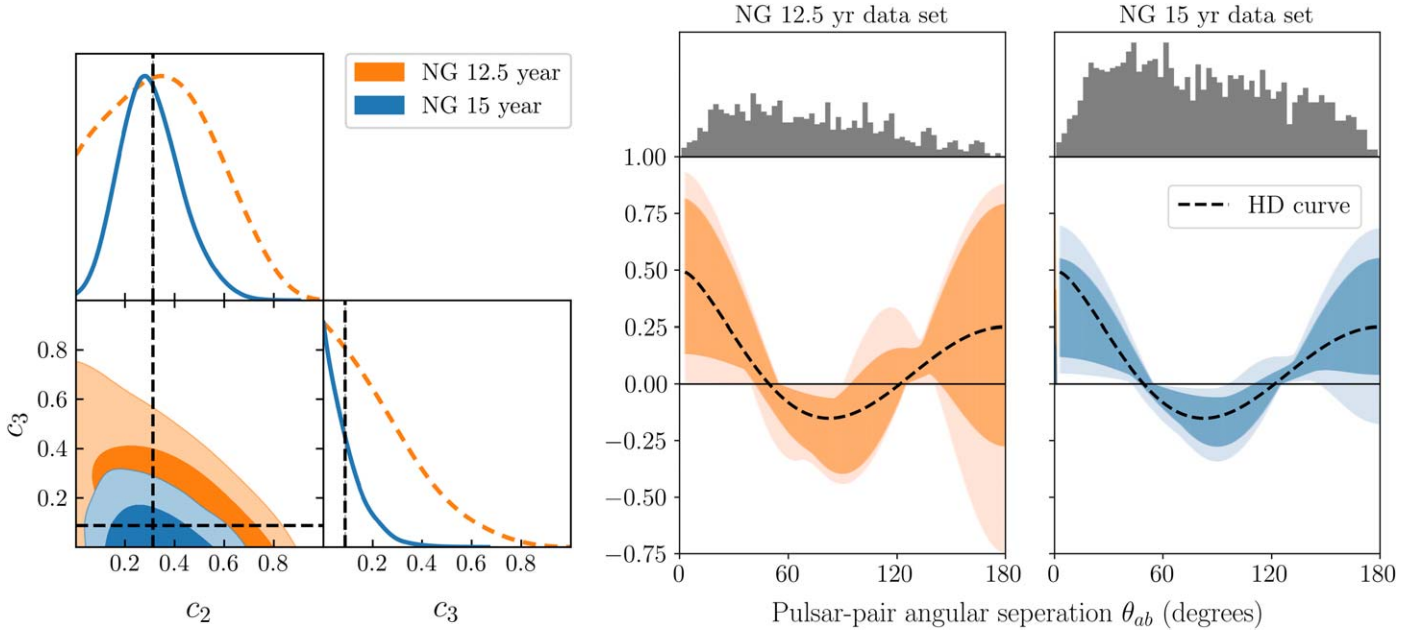


Figure 2. Left panel: marginalized 1D and 2D posterior distributions of c_2 and c_3 for the harmonic analysis $\text{HA}^\gamma(c_2, c_3)$ of the NANOGrav 12.5 and 15 yr data sets. The dashed black lines show the HD value of each Legendre coefficient. Right panel: reconstructed angular-correlation function from the same $\text{HA}^\gamma(c_2, c_3)$ model with the NANOGrav 12.5 and 15 yr data sets. The dark- and light-shaded regions denote the 68% and 95% CL regions, respectively, from the marginalized 2D posterior distributions of the quadrupole and octupole parameters shown in the left panel. The dashed black line is the HD curve, obtained from Equation (7). At the top of each plot, we provide a histogram of the pulsar pairs per angular separation bin for these two NANOGrav data sets.

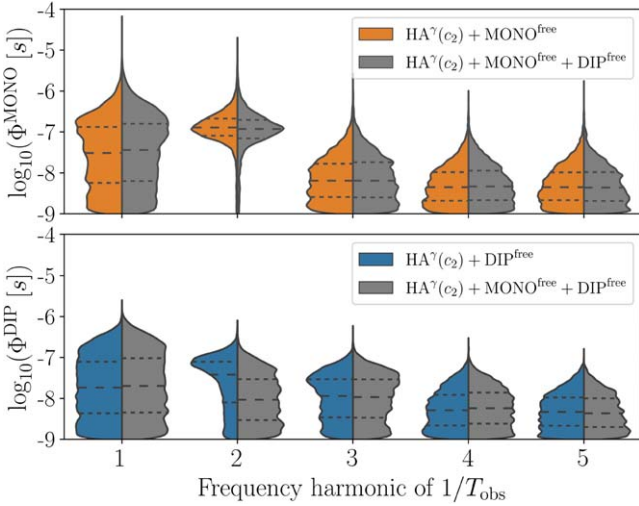


Figure 3. Marginalized 1D posterior distributions for the monopole (top plot) and dipole (bottom plot) free-spectrum parameters $\log_{10}\Phi_i$ of the first five frequency components $f_i = i/T_{\text{obs}}$ where $i = 1, \dots, 5$. The green (right-hand) portion of the split violin plots shows the results from a model that includes both monopole and dipole free-spectrum models. For the **NG15** data set, $T_{\text{obs}} = 16.03$ yr, which gives frequency components as multiples of ≈ 2 nHz.

we stress that the error bars in Figure 7 of **NG15** do not include the uncertainty in the estimator itself.

In addition to this, the assumption of a weak signal already breaks down for the **NG15**. Thus, the uncertainty in the MCOS is inherently an underestimate of the true uncertainty in the shape of the angular cross-correlations (K. A. Gersbach et al. 2025). Neglecting the pulsar-pair cross-correlations can underestimate the uncertainty by 20%–40% (G. Agazie et al. 2023a).

To directly compare the MCOS results with our work, we show the results of an analysis that includes the monopole, c_0 ,

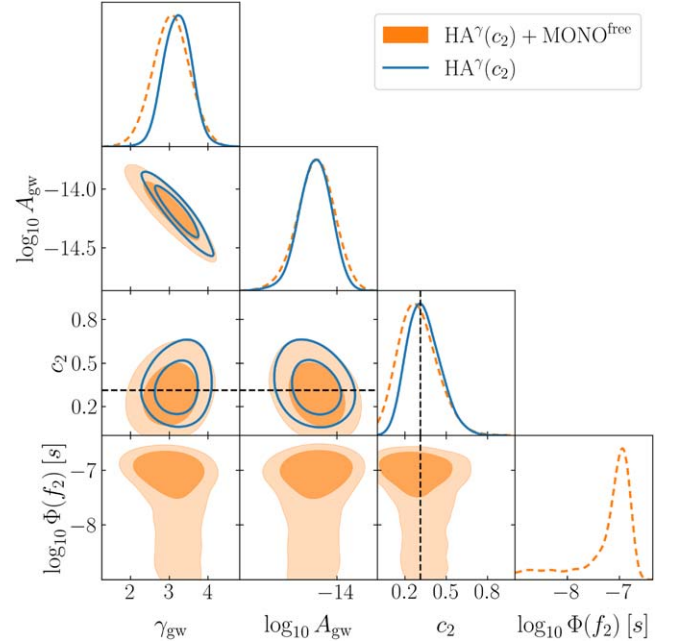


Figure 4. Marginalized 1D and 2D posterior distributions for a GWB analysis with monopole and quadrupole coefficients for the model $\text{HA}^\gamma(c_2) + \text{MONO}^{\text{free}}$ (shown as orange regions and dotted orange curves), overlaid with a quadrupole-only GWB analysis for the model $\text{HA}(c_2)$ (shown as solid blue curves). The monopole free-spectrum parameter $\log_{10}\Phi$ is associated with the second frequency bin ($f_2 = 2/T_{\text{obs}} \approx 4$ nHz). The full model includes monopole free-spectrum parameters from the 1st through 5th frequency bins. The dashed black line shows the HD value of the quadrupole coefficient.

dipole, c_1 , and quadrupole, c_2 , in the solid curves in Figure 5. It is important to note that the harmonic analysis approach requires Legendre coefficients to be positive (given that the angular power spectrum is positive) and the sum of Legendre

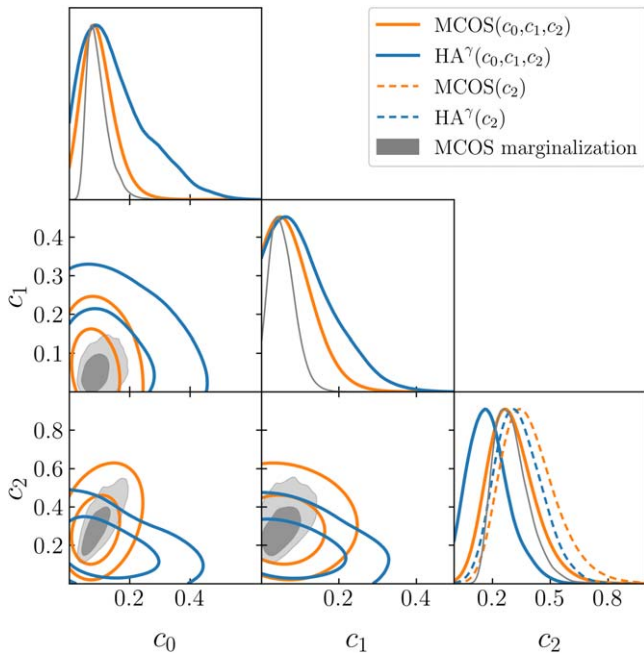


Figure 5. Marginalized 1D and 2D posterior distributions of frequentist MCOS and Bayesian harmonic analysis models with parameters c_0 , c_1 , and c_2 . The gray curves show the MCOS analysis that appears in NG15. The uncertainty in this analysis solely comes from marginalizing over the CURN⁷ parameters. The orange curves show the MCOS results when marginalizing over both the CURN⁷ parameters and the estimator uncertainty, as outlined in K. A. Gersbach et al. (2025). We do not include pulsar-pair covariance uncertainty for the MCOS results. The blue curves show the results of a harmonic analysis. The additional dashed curves in the 1D marginalized constraints on c_2 show c_2 -only analyses, as indicated in the figure legend.

coefficients to be less than 1 (to maintain a positive definite GWB covariance matrix), whereas there is no constraint on the prior range of the c_ℓ coefficients in the MCOS approach. We only show positive values for the MCOS results for simplicity. The gray lines and contours show the MCOS posteriors when only accounting for the uncertainty in the autocorrelations, whereas the orange lines and contours include both uncertainty in the autocorrelations as well as the estimator uncertainty, following the prescription outlined in K. A. Gersbach et al. (2025). The blue contours show the result of the harmonic analysis presented here. In order to cast the MCOS results in terms of the multipoles, we rescale the MCOS values by the value of A_{gw}^2 obtained from the same point in the CURN⁷ analysis chain.

In Figure 5, we also overlay the MCOS and harmonic analysis marginalized 1D posterior distribution for a c_2 -only model, shown as dashed curves. We see that the monopole coefficient has a larger impact on the posterior of the quadrupole for the harmonic analysis, compared to the MCOS approach. This is due to the fact that, as evident in the figure, the MCOS shows a positive correlation between c_0 and c_2 (correlation coefficient of ≈ 0.7), whereas the harmonic analysis shows a slight negative correlation (correlation coefficient of ≈ -0.3). Intuitively, we expect the correlation to be negative: to keep the overall amplitude of the cross-correlations approximately constant, an increase in one of these coefficients would have to be accompanied by a decrease in the other.

We stress that the harmonic analysis presented here does not suffer from any of the issues identified for the MCOS: the

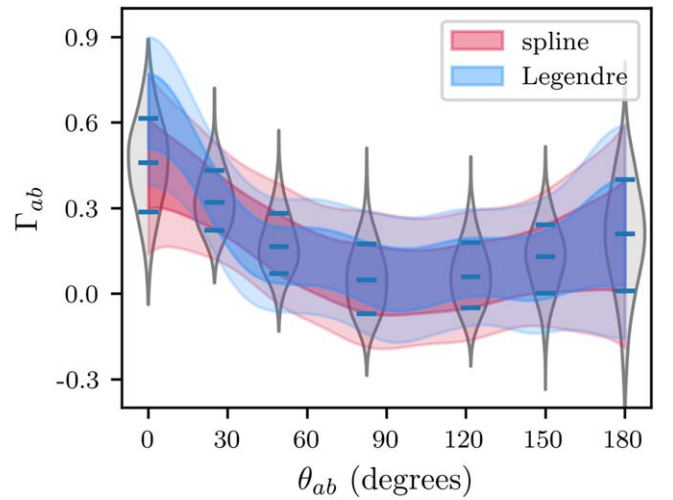


Figure 6. Comparison between constraints on the angular-correlation function using a binned function (S. R. Taylor et al. 2013; gray violins and red band) and the Legendre polynomial expansion $\text{HA}^\gamma(c_0, \dots, c_6)$ (J. Nay et al. 2024). The bands were constructed by drawing a large number of samples from the respective MCMCs and then computing the 1 and 2σ regions as a function of the angular separation. The dashed black curve is the HD function.

harmonic analysis directly utilizes the PTA likelihood and does not make any assumptions about the relative amplitude of the cross-correlations, and the posterior distributions automatically take all sources of uncertainty into account.

Finally, we compare our results to another Bayesian analysis approach used in both NG12.5 and NG15: an MCMC spline analysis, which fits a splined angular-correlation function to the data using seven spline knots. The choice of these spline-knot positions is based on important features of the theoretical HD curve: the end points, the zero crossings, the minimum, and two points between the end points and the zero crossings (S. R. Taylor et al. 2013). Just as in the harmonic analysis, the spline analysis fixes the correlation at $\theta_{ab} = 0$ to unity, effectively separating the autocorrelations from the cross-correlations (S. R. Taylor et al. 2013). Since there are seven spline knots, we compare the spline analysis to the harmonic analysis $\text{HA}^\gamma(c_0, \dots, c_6)$.

The MCMC spline analysis discussed in Section 3 of NG15 provides similar information to our constraints on the multipoles. In addition to having the same number of additional parameters, this harmonic analysis models variations in the correlations on the same angular scales. We show a comparison between these analyses in Figure 6 and find that both methods are consistent with each other. Moreover, Figure 6 indicates that the nonzero constraining power of the parameterized Γ_{ab} angular-correlation function comes predominantly from pulsar pairs separated by $\lesssim 30^\circ$.

5. Discussion and Conclusions

In this paper, we extend the work of NG15 to further characterize the angular correlations in the NANOGrav 15 yr data set using the harmonic analysis method from J. Nay et al. (2024). Our results show that the Bayesian evidence for quadrupole-only correlation models is consistent with the evidence for the HD model found in NG15 (i.e., the Bayes factor comparing these two models is approximately 1). We do not see evidence for multipoles higher than the quadrupole, which is expected due to the sharp drop-off in multipole

strength predicted by GR. We find the HD value of the quadrupole coefficient falls within the 68% CL of the measured quadrupole’s marginalized 1D posterior distribution, $c_2/c_2^{\text{HD}} = 1.088^{+0.32}_{-0.45}$. We reconstruct the angular-correlation function from the posterior distributions for c_2 and c_3 and find that the measurements are consistent with the angular correlations of the HD curve.

We show that the large jump in quadrupole evidence between the NG12.5 and NG15 data sets is primarily due to the increase in the observation time, which is consistent with a GWB frequency power spectrum that increases in strength at decreasing frequencies. This result is consistent with the expected scaling of the marginalized 1D posterior distribution mean-to-standard deviation ratio of the quadrupole with time versus number of pulsars found in J. Nay et al. (2024). The current mean-to-standard deviation ratio of the quadrupole is ~ 2.5 ; using the scaling found in J. Nay et al. (2024), we expect to have a similar mean-to-standard deviation ratio of the octupole within roughly 10 yr.

Previous work in determining the shape of the measured angular correlations has either used a binned estimator of the correlations between pairs of pulsars (MCOS) or placed constraints on a spline parameterization of the angular correlations. Both of these approaches give broadly similar results to what we have found, but also present some challenges when trying to interpret them. In particular, the MCOS results presented in NG15 neglect cross-correlations between different pairs of pulsars, leading to an underestimate of the resulting uncertainty, and constraints on the amplitude of the knots of the spline analysis are highly correlated with one another. We note that recent work on improving the frequentist estimator has included all pulsar cross-correlations, but that this has yet to be applied to providing constraints on the shape of the angular correlations (K. A. Gersbach et al. 2025).

When we include a monopole free-spectrum model in our harmonic analysis, the evidence of the quadrupole correlation is reduced by more than an order of magnitude due to the presence of a monopolar signal at ≈ 4 nHz. This monopolar signal has been investigated in detail, which we briefly summarize below. Clock errors can cause monopole correlations (C. Tiburzi et al. 2016; Z. Arzoumanian et al. 2020), but extensive investigations by NANOGrav have shown no evidence of this type of systematic error (see discussion in Section 5.3 of NG15). Other possible explanations include GWs from an individual SMBHB source (G. Agazie et al. 2023d), ultralight dark matter (A. Afzal et al. 2023), and additional or alternate GW polarization modes (G. Agazie et al. 2024). To date, none of these additional investigations have been able to explain the source of the monopolar signal. As stated in NG15, if this monopolar signal is due to an astrophysical or cosmological source, then its persistence in future data sets will help determine the source of the signal. We also note that, to date, it is unclear whether the other PTA data sets are consistent with this monopolar signal (see, e.g., J. Antoniadis et al. 2023), and we leave such an analysis to future work.

Our choice of parameterizing the angular correlations through Legendre polynomials is not unique—any set of complete functions can be used. For example, it is possible to develop a set of functions that are statistically uncorrelated with the HD function (often referred to as “principal components”; D. R. Madison 2024). An analysis that uses these functions

may be better suited to more clearly identify potential deviations from the expected angular correlations. However, given that the expected angular power spectrum is predominantly quadrupolar, a Legendre polynomial expansion is the natural choice when assessing the Bayesian evidence for angular correlations.

As our PTA data sets improve, it will be imperative to have multiple techniques to characterize the frequency and angular information contained within them. A confirmation of the standard expectations will lend credence to the interpretation that the GWB observed by PTAs is generated by a cosmological collection of SMBHBs generating tensor GWs that propagate at the speed of light. Even within this paradigm, we expect deviations due to the fact that the SMBHBs form a finite population that clusters on cosmological scales. Deviations from the standard expectations may provide evidence for unexpected dynamics in the SMBHB population, modifications to GR, and/or the presence of exotic GW sources such as cosmic strings or early universe phase transitions (see, e.g., A. Afzal et al. 2023). The confirmation that the currently measured angular correlations in the NG15 data set are largely consistent with standard expectations—though with hints of a possible monopole—is just a first step into a very exciting future.

Acknowledgments

The work contained herein has been carried out by the NANOGrav collaboration, which receives support from the National Science Foundation (NSF) Physics Frontier Center award Nos. 1430284 and 2020265, the Gordon and Betty Moore Foundation, NSF AccelNet award No. 2114721, an NSERC Discovery Grant, and CIFAR. The Arecibo Observatory is a facility of the NSF operated under cooperative agreement (AST-1744119) by the University of Central Florida (UCF) in alliance with Universidad Ana G. Méndez (UAGM) and Yang Enterprises (YEI), Inc. The Green Bank Observatory is a facility of the NSF operated under cooperative agreement by Associated Universities, Inc. K.K.B. and J.E.N. acknowledge the Texas Advanced Computing Center (TACC) at The University of Texas at Austin for providing high-performance computing resources that contributed to the analyses reported within this paper. T.L.S. acknowledges the Strelka Computing Cluster run by Swarthmore College that contributed to the analyses reported within this paper. L.B. acknowledges support from the National Science Foundation under award AST-1909933 and from the Research Corporation for Science Advancement under Cottrell Scholar Award No. 27553. P.R.B. is supported by the Science and Technology Facilities Council, grant No. ST/W000946/1. S.B. gratefully acknowledges the support of a Sloan Fellowship and the support of NSF under award #1815664. The work of R.B., R.C., D.D., N.L., X.S., J. P.S., and J.A.T. is partly supported by the George and Hannah Bolinger Memorial Fund in the College of Science at Oregon State University. M.C., P.P., and S.R.T. acknowledge support from NSF AST-2007993. M.C. and N.S.P. were supported by the Vanderbilt Initiative in Data Intensive Astrophysics (VIDA) Fellowship. K.C., A.D.J., and M.V. acknowledge support from the Caltech and Jet Propulsion Laboratory President’s and Director’s Research and Development Fund. K.C. and A.D.J. acknowledge support from the Sloan Foundation. Support for this work was provided by the NSF through the Grote Reber Fellowship Program administered by Associated Universities,

Inc./National Radio Astronomy Observatory. Support for H.T. C. is provided by NASA through the NASA Hubble Fellowship Program grant #HST-HF2-51453.001 awarded by the Space Telescope Science Institute, which is operated by the Association of Universities for Research in Astronomy, Inc., for NASA, under contract NAS5-26555. K.C. is supported by a UBC Four Year Fellowship (6456). M.E.D. acknowledges support from the Naval Research Laboratory by NASA under contract S-15633Y. T.D. and M.T.L. were supported by an NSF Astronomy and Astrophysics grant (AAG) award No. 2009468. E.C.F. is supported by NASA under award No. 80GSFC21M0002. G.E.F., S.C.S., and S.J.V. are supported by NSF award PHY-2011772. K.A.G. and S.R.T. acknowledge support from an NSF CAREER award #2146016. The Flatiron Institute is supported by the Simons Foundation. S.H. is supported by the National Science Foundation Graduate Research Fellowship under grant No. DGE-1745301. N.L. acknowledges the support from Larry W. Martin and Joyce B. O’Neill Endowed Fellowship in the College of Science at Oregon State University. Part of this research was carried out at the Jet Propulsion Laboratory, California Institute of Technology, under a contract with the National Aeronautics and Space Administration (80NM0018D0004). D.R.L. and M.A.M. are supported by NSF #1458952. M.A.M. is supported by NSF #2009425. C.M.F.M. was supported in part by the National Science Foundation under grants No. NSF PHY-1748958 and AST-2106552. A.M. is supported by the Deutsche Forschungsgemeinschaft under Germany’s Excellence Strategy—EXC 2121 Quantum Universe—390833306. The Dunlap Institute is funded by an endowment established by the David Dunlap family and the University of Toronto. K.D.O. was supported in part by NSF grant No. 2207267. T.T.P. acknowledges support from the Extragalactic Astrophysics Research Group at Eötvös Loránd University, funded by the Eötvös Loránd Research Network (ELKH), which was used during the development of this research. S.M.R. and I.H.S. are CIFAR Fellows. Portions of this work were performed at NRL and were supported by ONR 6.1 basic research funding. J.S. is supported by an NSF Astronomy and Astrophysics Postdoctoral Fellowship under award AST-2202388 and acknowledges previous support by the NSF under award 1847938. C.U. acknowledges support from BGU (Kreitman fellowship), and the Council for Higher Education and the Israel Academy of Sciences and Humanities (Excellence fellowship). C.A.W. acknowledges support from CIERA, the Adler Planetarium, and the Brinson Foundation through a CIERA-Adler postdoctoral fellowship. O.Y. is supported by the National Science Foundation Graduate Research Fellowship under grant No. DGE-2139292.

Author Contributions

An alphabetical-order author list was used for this paper in recognition of the fact that a large, decade-timescale project such as NANOGrav is necessarily the result of the work of many people. All authors contributed to the activities of the NANOGrav collaboration leading to the work presented here and reviewed the manuscript, text, and figures prior to the paper’s submission. Additional specific contributions to this paper are as follows.

J.E.N. wrote and developed new Python codes to perform the analysis, created figures and tables, and wrote a majority of the text. T.L.S. made significant contributions to the text, ran some of the analyses, and created some of the figures. K.K.B.,

T.L.S., and C.M.F.M. conceived of the project, supervised the analysis, helped write and develop the manuscript, and provided advice on figures and interpretation. A.S. provided insights into the analysis, helped interpret the results, and provided comments on the manuscript.

G.A., A.A., A.M.A., Z.A., P.T.B., P.R.B., H.T.C., K.C., M.E.D., P.B.D., T.D., E.C.F., W.F., E.F., G.E.F., N.G., P.A.G., J.G., D.C.G., J.S.H., R.J.J., M.L.J., D.L.K., M.K., M.T.L., D.R.L., J.L., R.S.L., A.M., M.A.M., N.M., B.W.M., C.N., D.J.N., T.T.P., B.B.P.P., N.S.P., H.A.R., S.M.R., P.S.R., A.S., C.S., B.J.S., I.H.S., K.S., A.S., J.K.S., and H.M.W. ran observations and developed timing models for the NG15 data set.

ORCID iDs

Gabriella Agazie  <https://orcid.org/0000-0001-5134-3925>
 Akash Anumarlapudi  <https://orcid.org/0000-0002-8935-9882>
 Anne M. Archibald  <https://orcid.org/0000-0003-0638-3340>
 Jeremy G. Baier  <https://orcid.org/0000-0002-4972-1525>
 Paul T. Baker  <https://orcid.org/0000-0003-2745-753X>
 Bence Bécsy  <https://orcid.org/0000-0003-0909-5563>
 Laura Blecha  <https://orcid.org/0000-0002-2183-1087>
 Kimberly K. Boddy  <https://orcid.org/0000-0003-1928-4667>
 Adam Brazier  <https://orcid.org/0009-0008-6187-8753>
 Paul R. Brook  <https://orcid.org/0000-0003-3053-6538>
 Sarah Burke-Spolaor  <https://orcid.org/0000-0003-4052-7838>
 J. Andrew Casey-Clyde  <https://orcid.org/0000-0002-5557-4007>
 Maria Charisi  <https://orcid.org/0000-0003-3579-2522>
 Shami Chatterjee  <https://orcid.org/0000-0002-2878-1502>
 Tyler Cohen  <https://orcid.org/0000-0001-7587-5483>
 James M. Cordes  <https://orcid.org/0000-0002-4049-1882>
 Neil J. Cornish  <https://orcid.org/0000-0002-7435-0869>
 Fronefield Crawford  <https://orcid.org/0000-0002-2578-0360>
 H. Thankful Cromartie  <https://orcid.org/0000-0002-6039-692X>
 Kathryn Crowter  <https://orcid.org/0000-0002-1529-5169>
 Megan E. DeCesar  <https://orcid.org/0000-0002-2185-1790>
 Paul B. Demorest  <https://orcid.org/0000-0002-6664-965X>
 Lankeswar Dey  <https://orcid.org/0000-0002-2554-0674>
 Timothy Dolch  <https://orcid.org/0000-0001-8885-6388>
 Elizabeth C. Ferrara  <https://orcid.org/0000-0001-7828-7708>
 William Fiore  <https://orcid.org/0000-0001-5645-5336>
 Emmanuel Fonseca  <https://orcid.org/0000-0001-8384-5049>
 Gabriel E. Freedman  <https://orcid.org/0000-0001-7624-4616>
 Emiko C. Gardiner  <https://orcid.org/0000-0002-8857-613X>
 Nate Garver-Daniels  <https://orcid.org/0000-0001-6166-9646>
 Peter A. Gentile  <https://orcid.org/0000-0001-8158-683X>
 Joseph Glaser  <https://orcid.org/0000-0003-4090-9780>
 Deborah C. Good  <https://orcid.org/0000-0003-1884-348X>
 Kayhan Gültekin  <https://orcid.org/0000-0002-1146-0198>
 Jeffrey S. Hazboun  <https://orcid.org/0000-0003-2742-3321>
 Ross J. Jennings  <https://orcid.org/0000-0003-1082-2342>
 Aaron D. Johnson  <https://orcid.org/0000-0002-7445-8423>
 Megan L. Jones  <https://orcid.org/0000-0001-6607-3710>
 David L. Kaplan  <https://orcid.org/0000-0001-6295-2881>
 Luke Zoltan Kelley  <https://orcid.org/0000-0002-6625-6450>
 Matthew Kerr  <https://orcid.org/0000-0002-0893-4073>
 Joey S. Key  <https://orcid.org/0000-0003-0123-7600>
 Nima Laal  <https://orcid.org/0000-0002-9197-7604>
 Michael T. Lam  <https://orcid.org/0000-0003-0721-651X>
 William G. Lamb  <https://orcid.org/0000-0003-1096-4156>
 Bjorn Larsen  <https://orcid.org/0000-0001-6436-8216>
 Natalia Lewandowska  <https://orcid.org/0000-0003-0771-6581>
 Tingting Liu  <https://orcid.org/0000-0001-5766-4287>

Duncan R. Lorimer  <https://orcid.org/0000-0003-1301-966X>
 Jing Luo  <https://orcid.org/0000-0001-5373-5914>
 Ryan S. Lynch  <https://orcid.org/0000-0001-5229-7430>
 Chung-Pei Ma  <https://orcid.org/0000-0002-4430-102X>
 Dustin R. Madison  <https://orcid.org/0000-0003-2285-0404>
 Alexander McEwen  <https://orcid.org/0000-0001-5481-7559>
 James W. McKee  <https://orcid.org/0000-0002-2885-8485>
 Maura A. McLaughlin  <https://orcid.org/0000-0001-7697-7422>
 Natasha McMann  <https://orcid.org/0000-0002-4642-1260>
 Bradley W. Meyers  <https://orcid.org/0000-0001-8845-1225>
 Patrick M. Meyers  <https://orcid.org/0000-0002-2689-0190>
 Chiara M. F. Mingarelli  <https://orcid.org/0000-0002-4307-1322>
 Andrea Mitridate  <https://orcid.org/0000-0003-2898-5844>
 Jonathan Nay  <https://orcid.org/0009-0006-8387-2040>
 Cherry Ng  <https://orcid.org/0000-0002-3616-5160>
 David J. Nice  <https://orcid.org/0000-0002-6709-2566>
 Stella Koch Ocker  <https://orcid.org/0000-0002-4941-5333>
 Ken D. Olum  <https://orcid.org/0000-0002-2027-3714>
 Timothy T. Pennucci  <https://orcid.org/0000-0001-5465-2889>
 Benetge B. P. Perera  <https://orcid.org/0000-0002-8509-5947>
 Polina Petrov  <https://orcid.org/0000-0001-5681-4319>
 Nihan S. Pol  <https://orcid.org/0000-0002-8826-1285>
 Henri A. Radovan  <https://orcid.org/0000-0002-2074-4360>
 Scott M. Ransom  <https://orcid.org/0000-0001-5799-9714>
 Paul S. Ray  <https://orcid.org/0000-0002-5297-5278>
 Jessie C. Runnoe  <https://orcid.org/0000-0001-8557-2822>
 Alexander Saffer  <https://orcid.org/0000-0001-7832-9066>
 Shashwat C. Sardesai  <https://orcid.org/0009-0006-5476-3603>
 Ann Schmiedekamp  <https://orcid.org/0000-0003-4391-936X>
 Carl Schmiedekamp  <https://orcid.org/0000-0002-1283-2184>
 Kai Schmitz  <https://orcid.org/0000-0003-2807-6472>
 Brent J. Shapiro-Albert  <https://orcid.org/0000-0002-7283-1124>
 Xavier Siemens  <https://orcid.org/0000-0002-7778-2990>
 Joseph Simon  <https://orcid.org/0000-0003-1407-6607>
 Magdalena S. Siwek  <https://orcid.org/0000-0002-1530-9778>
 Tristan L. Smith  <https://orcid.org/0000-0003-2685-5405>
 Sophia V. Sosa Fiscella  <https://orcid.org/0000-0002-5176-2924>
 Ingrid H. Stairs  <https://orcid.org/0000-0001-9784-8670>
 Daniel R. Stinebring  <https://orcid.org/0000-0002-1797-3277>
 Kevin Stovall  <https://orcid.org/0000-0002-7261-594X>
 Abhimanyu Susobhanan  <https://orcid.org/0000-0002-2820-0931>
 Joseph K. Swiggum  <https://orcid.org/0000-0002-1075-3837>
 Stephen R. Taylor  <https://orcid.org/0000-0003-0264-1453>
 Jacob E. Turner  <https://orcid.org/0000-0002-2451-7288>
 Caner Unal  <https://orcid.org/0000-0001-8800-0192>
 Michele Vallisneri  <https://orcid.org/0000-0002-4162-0033>
 Rutger van Haasteren  <https://orcid.org/0000-0002-6428-2620>
 Sarah J. Vigeland  <https://orcid.org/0000-0003-4700-9072>
 Haley M. Wahl  <https://orcid.org/0000-0001-9678-0299>
 Caitlin A. Witt  <https://orcid.org/0000-0002-6020-9274>
 David Wright  <https://orcid.org/0000-0003-1562-4679>
 Olivia Young  <https://orcid.org/0000-0002-0883-0688>

References

Afzal, A., Agazie, G., Anumarlapudi, A., et al. 2023, *ApJL*, 951, L11
 Agazie, G., Anumarlapudi, A., Archibald, A. M., et al. 2023a, *ApJL*, 951, L8
 Agazie, G., Anumarlapudi, A., Archibald, A. M., et al. 2023b, *ApJL*, 952, L37
 Agazie, G., Anumarlapudi, A., Archibald, A. M., et al. 2023c, *ApJL*, 951, L10

Agazie, G., Anumarlapudi, A., Archibald, A. M., et al. 2023d, *ApJL*, 951, L50
 Agazie, G., Anumarlapudi, A., Archibald, A. M., et al. 2024, *ApJL*, 964, L14
 Ali-Haïmoud, Y., Smith, T. L., & Mingarelli, C. M. F. 2020, *PhRvD*, 102, 122005
 Allen, B., Dhurandhar, S., Gupta, Y., et al. 2023, arXiv:2304.04767
 Anholm, M., Ballmer, S., Creighton, J. D. E., Price, L. R., & Siemens, X. 2009, *PhRvD*, 79, 084030
 Antoniadis, J., Arzoumanian, Z., Babak, S., et al. 2022, *MNRAS*, 510, 4873
 Antoniadis, J., Arumugam, P., Arumugam, S., et al. 2023, *A&A*, 678, A50
 Arzoumanian, Z., Brazier, A., Burke-Spolaor, S., et al. 2015, *ApJ*, 813, 65
 Arzoumanian, Z., Baker, P. T., Blumer, H., et al. 2020, *ApJL*, 905, L34
 Arzoumanian, Z., Baker, P. T., Blumer, H., et al. 2021, *ApJL*, 923, L22
 Boddy, K. K., Lisanti, M., McDermott, S. D., et al. 2022, *JHEAp*, 35, 112
 Caldwell, R., Cui, Y., Guo, H., et al. 2022, *GReGr*, 54, 156
 Carlin, B. P., & Chib, S. 2018, *J. R. Stat. Soc. Ser. B Methodol.*, 57, 473
 Chamberlin, S. J., Creighton, J. D. E., Siemens, X., et al. 2015, *PhRvD*, 91, 044048
 Chamberlin, S. J., & Siemens, X. 2012, *PhRvD*, 85, 082001
 Chen, S., Caballero, R. N., Guo, Y. J., et al. 2021, *MNRAS*, 508, 4970
 Cornish, N. J., O’Beirne, L., Taylor, S. R., & Yunes, N. 2018, *PhRvL*, 120, 181101
 Demorest, P. B., Ferdman, R. D., Gonzalez, M. E., et al. 2013, *ApJ*, 762, 94
 Detweiler, S. L. 1979, *ApJ*, 234, 1100
 Dickey, J. M. 1971, *Ann. Math. Stat.*, 42, 204
 Ellis, J., & van Haasteren, R. 2017, jellis18/PTMCMCSampler: Official Release v1.0.0, Zenodo, doi:10.5281/zenodo.1037579
 Ellis, J. A., Vallisneri, M., Taylor, S. R., & Baker, P. T. 2020, ENTERPRISE: Enhanced Numerical Toolbox Enabling a Robust Pulsar Inference Suite v3.0.0, Zenodo, doi:10.5281/zenodo.4059815
 Gair, J., Romano, J. D., Taylor, S., & Mingarelli, C. M. F. 2014, *PhRvD*, 90, 082001
 Gelman, A., & Rubin, D. B. 1992, *StaSc*, 7, 457
 Gersbach, K. A., Taylor, S. R., Meyers, P. M., & Romano, J. D. 2025, *PhRvD*, 111, 023027
 Godsil, S. J. 2001, *J. Computational and Graphical Statistics*, 10, 230
 Goncharov, B., Shannon, R. M., Reardon, D. J., et al. 2021, *ApJL*, 917, L19
 Green, D., Ruderman, J. T., Safdi, B. R., et al. 2022, arXiv:2209.06854
 Hee, S., Handley, W., Hobson, M. P., & Lasenby, A. N. 2016, *MNRAS*, 455, 2461
 Hellings, R. W., & Downs, G. S. 1983, *ApJL*, 265, L39
 Hobbs, G., Coles, W., Manchester, R. N., et al. 2012, *MNRAS*, 427, 2780
 Hobbs, G., Guo, L., Caballero, R. N., et al. 2019, *MNRAS*, 491, 5951
 Hotinli, S. C., Kamionkowski, M., & Jaffe, A. H. 2019, *OJAp*, 2, 8
 Jeffreys, H. 1998, *The Theory of Probability* (3rd ed.; Oxford: Oxford Univ. Press)
 Johnson, A. D., Meyers, P. M., Baker, P. T., et al. 2024, *PhRvD*, 109, 103012
 Jones, M. L., McLaughlin, M. A., Lam, M. T., et al. 2017, *ApJ*, 841, 125
 Lee, K. J., Jenet, F. A., & Price, R. H. 2008, *ApJ*, 685, 1304
 Madison, D. R. 2024, *PhRvD*, 110, 104066
 Maggiore, M. 2018, *Gravitational Waves. Vol. 2: Astrophysics and Cosmology* (Oxford: Oxford Univ. Press)
 Matsakis, D. N., Taylor, J. H., & Eubanks, T. M. 1997, *A&A*, 326, 924
 Mingarelli, C. M. F., & Casey-Clyde, J. A. 2022, *Sci*, 378, 592
 Mingarelli, C. M. F., Sidery, T., Mandel, I., & Vecchio, A. 2013, *PhRvD*, 88, 062005
 Nay, J., Boddy, K. K., Smith, T. L., & Mingarelli, C. M. F. 2024, *PhRvD*, 110, 044062
 Phinney, E. S. 2001, arXiv:astro-ph/0108028
 Qin, W., Boddy, K. K., Kamionkowski, M., & Dai, L. 2019, *PhRvD*, 99, 063002
 Reardon, D. J., Zic, A., Shannon, R. M., et al. 2023, *ApJL*, 951, L6
 Roebber, E. 2019, *ApJ*, 876, 55
 Roebber, E., & Holder, G. 2017, *ApJ*, 835, 21
 Sardesai, S. C., Vigeland, S. J., Gersbach, K. A., & Taylor, S. R. 2023, *PhRvD*, 108, 124081
 Sazhin, M. V. 1978, *SvA*, 36, 22
 Taylor, S. R., Baker, P. T., Hazboun, J. S., Simon, J., & Vigeland, S. J. 2021, enterprise-extensions, https://github.com/nanograv/enterprise_extension
 Taylor, S. R., & Gair, J. R. 2013, *PhRvD*, 88, 084001
 Taylor, S. R., Gair, J. R., & Lentati, L. 2013, *PhRvD*, 87, 044035
 Tiburzi, C., Hobbs, G., Kerr, M., et al. 2016, *MNRAS*, 455, 4339
 Vallisneri, M., Taylor, S. R., Simon, J., et al. 2020, *ApJ*, 893, 112
 Vigeland, S. J., Iso, K., Taylor, S. R., & Ellis, J. A. 2018, *PhRvD*, 98, 044003
 Xu, H., Chen, S., Guo, Y., et al. 2023, *RAA*, 23, 075024